

**Semi-Analytical Treatment of Wall Heat Transfer
Coupled to a Numerical Simulation Model of Fire**

A. Horvat¹, Y. Sinai, P. Tofilo

Keywords: conjugate heat transfer, fire simulation, transient, semi-analytical methods

Abstract

The analysis focuses on the importance of accurate description of walls' thermal behaviour with particularly relevance to fire safety cases. To accurately predict thermal loads on the walls in a complex fire situation, time dependent phenomena of thermal convection, diffusion, radiation and heat transfer across the wall have to be taken into account. The heat transfer across the walls is often neglected as it requires fine grid resolution to approximate large temperature gradients. The analysis shows that this can lead to substantial errors and proposes a transient semi-analytical approximation of thermal wall behaviour. Unsteady heat diffusion equation is solved by semi-analytical approximation of a temperature profile in a wall. The temperature profile is approximated in each time step and for each wall grid node separately using the temperature at the wall internal side and Biot number at the external side for boundary conditions. Wall heat transfer coefficient is calculated as a temperature profile derivative and then used in the coupled numerical model of the fire. The semi-analytical approach does not rely on a discretisation procedure and the accuracy of its solutions is independent of grid spacing. Therefore, such semi-analytical technique is computationally less expensive and especially attractive for long transient calculations.

¹ corresponding author

Nomenclature

Latin letters

A, B	constants
a, b	multigrey gas model coefficients
dt	timestep
Bi_{out}	Biot number ($= h_{out} \delta / k_w$)
D	kinematic mass diffusivity
C_A	coefficient of eddy dissipation combustion model
F_1, F_2	SST model function
G	turbulence production due to buoyancy
g	gravitational acceleration, grey gas
h	enthalpy
I	radiation intensity
$J^{(1)}, J^{(2)}$	integrals
K	radiation coefficient
k	turbulence kinetic energy
P	turbulence production due to stresses
p	pressure
Pr_t	turbulent Prandtl number ($= 0.9$)
q	heat flux
R	reaction rate
r	spatial dependence
s	path length
S	source term
Sc_t	turbulent Schmidt number ($=0.9$)
T	temperature
t	time, time scale
v	velocity
x	spatial coordinate

Greek letters

α_1, α_3	SST model parameter
β^*, β_3	SST model parameters
δ	Kronecker delta function, wall thickness
ε	eddy dissipation rate

ζ	molecular concentration
θ	angle
ϑ	thermal diffusivity
λ	wave length, eigenvalues
μ	dynamic viscosity
ν	stoichiometric coefficients
ξ	mass fraction
ρ	density
$\sigma_{\omega 2}, \sigma_{k 3}, \sigma_{\omega 3}$	SST model parameters
Ψ	volume fraction
φ	angle
Ω	angle
ω	eddy frequency

Subscripts/superscripts

<i>a</i>	absorption
<i>b</i>	blackbody
<i>c</i>	component, convective
<i>comb</i>	combustion
<i>e</i>	emitted radiation
<i>env</i>	environment
<i>g</i>	gauge
<i>gas</i>	gaseous phase
<i>i</i>	irradiation
<i>in</i>	internal wall
<i>n</i>	timestep
<i>out</i>	external wall
<i>r</i>	reflected radiation
<i>rad</i>	radiation
<i>ref</i>	reference state
<i>s</i>	scattering
<i>stat</i>	static
<i>t</i>	turbulence
<i>w</i>	wall

Symbols

'	fluctuation from a time average
-	time average
^	dimensionless variable

1. Introduction

The aim of this paper is to present a computational technique for prediction of transient compartment fires that incorporates numerical simulation of mass, momentum and heat transport as well as a semi-analytical calculation of heat transfer across the walls. The investigation is a part of FIRENET project, which main goal is to advance understanding and predictive capabilities of under-ventilated fires. The presented methodology is tested for a case of fire in an enclosure with an opening (Figure 1). The size and position of the opening control availability of oxygen for the combustion process. In such case, the fire and, consequently, the released heat are especially sensitive to local distribution of velocity, concentrations and temperature; the fire is ventilation controlled. The presented computational case is only one of many that were studied experimentally by Tofilo et al. [1]. Their objective was to assess the influence of ventilation factor and fire sootiness on wall heat flux and temperature distribution.

In the combustion and fire modelling community, significant research effort is being invested in improvements of combustion kinetics, usually in combination with advanced turbulence modelling (e.g. Jaber and James [2], Jiang and Luo [3], Hilbert et al. [4]). Large-eddy simulation (LES) and direct numerical simulation (DNS) are becoming more and more popular. Although, they provide a useful research tool for numerical studies, these methods are computationally very demanding and therefore with few exceptions (Janicka and Sadiki, [5]) not suitable for large industrial and environmental applications. Hybrid methods (Koutmos et al. [6]) that incorporate Reynolds averaged transport equations in wall proximity and large-eddy simulation models in bulk of the flow are much more relevant for practical use. Recent reviews of fire modelling practice may be found in Kumar and Cox [7] and Gobeau et al. [8]. A review of industrial applications has been provided by Stopford [9].

Although current fire research covers many aspect of the phenomenon, this paper focuses on the importance of accurate description of walls' thermal behaviour. In some engineering applications, this is an important question which determines structural damage and failure, time to structural collapse, and is of particularly relevance to fire safety measures (e.g. Yeoh et al. [10]). To successfully predict thermal loads on the walls in a complex fire situation, one has to take into account time dependent phenomena of thermal convection, diffusion and radiation as well as heat transfer across the wall. The latter effect is often unjustly neglected

as it requires fine grid resolution across thin walls. Due to high temperature gradients that need to be resolved, this part of computation may well be can computationally most expensive. The common approximations are

- a. steady-state (resistances in series) (Holman [11]),
- b. ‘eddy penetration’ approximation (Drysedale [12], Carslaw and Jaeger [13]),
- c. ‘lumped parameter’ (Holman [11]).

The authors present a transient semi-analytical technique for solving time dependent heat conduction problem in the walls. As the numerical finite volume code solves the fluid transport equations, the coupled semi-analytical algorithm simultaneously calculates the temperature profile in the walls for each integration time step. Steady-state computations of complex conjugate heat transfer problems were reported in the past (e.g. Horvat and Catton [14], Horvat and Mavko [15]), whereas applications of transient semi-analytical methods in combination with numerical codes have been rare. Nevertheless, a method based on Fredholm integrals was employed by Chernyshov [16], and a similar approach to ours has been recently outlined by Pruess and Zhang [17] for modelling wellbore heat transmission. They use a series of polynomial functions to construct the temperature profile in the layers, whereas our solution is a combination of linear function and a series of sinusoidal functions.

2. Numerical model of a fire

The numerical model (Figure 1) closely followed the experimental test section of Tofilo et al. [1] that corresponds to 1/3 the ISO room size. It is 1.2 m long, 0.8 m wide and 0.8 m high. The walls and ceiling had an inner layer of 25 mm thick insulation board (Fiberfax LD Duraboard) and outer layer of 10 mm thick fire retarded chipboard. The floor was made of high density fibreboard.

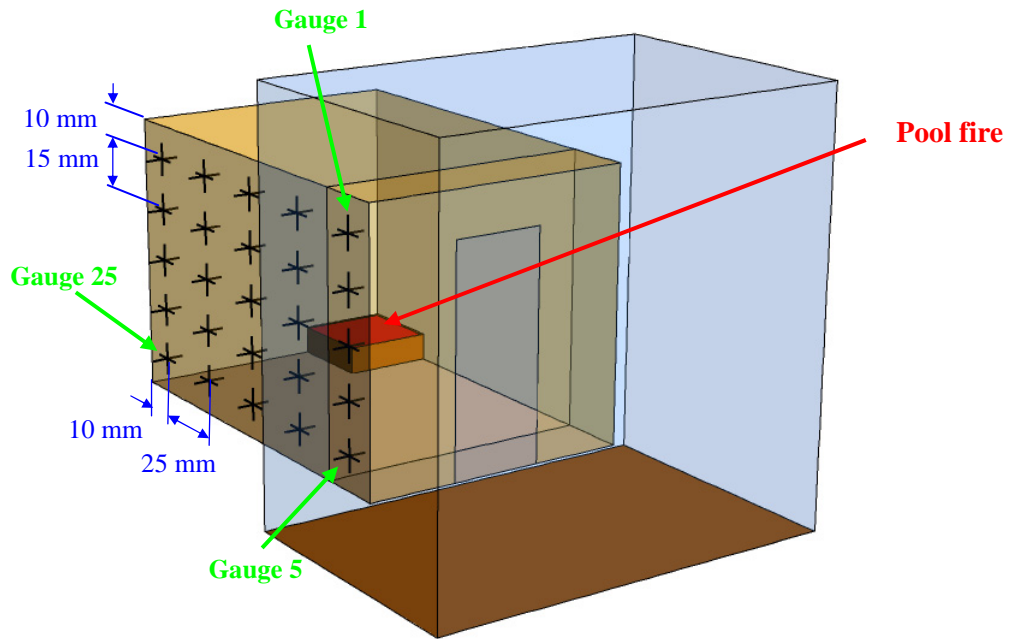


Figure 1: Simulation domain of the CFD model with the location of heat flux (steel plates) measuring points

As in the experiments, methanol was used as a fuel. The fuel source at the back left corner of the enclosure was represented with an inlet boundary, 0.25 m by 0.25 m in size and elevated for 8 cm. The experimentally recorded fuel mass loss is given in Figure 2. It was directly applied as the inlet boundary condition in the numerical simulations.

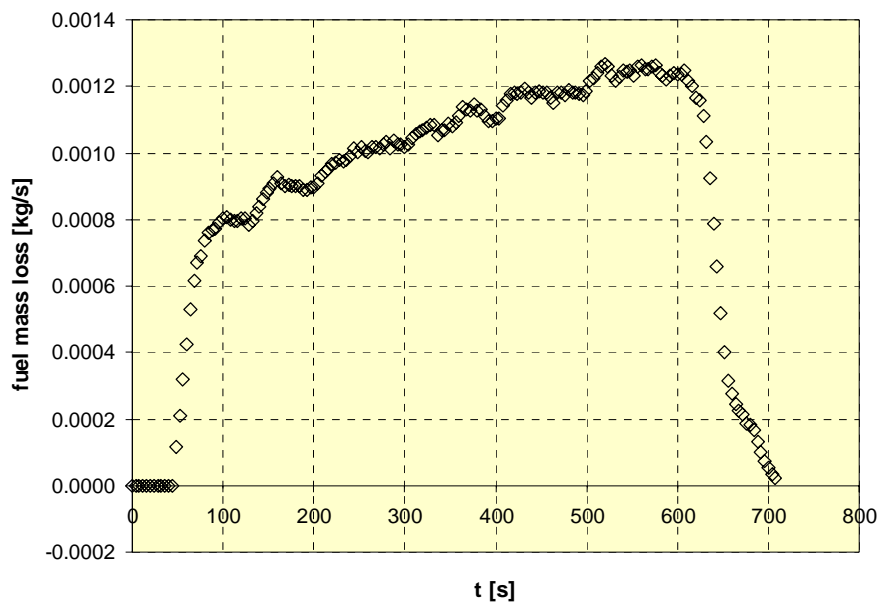


Figure 2 : Fuel mass loss as recorded in the experiment (Tofilo et al. [1])

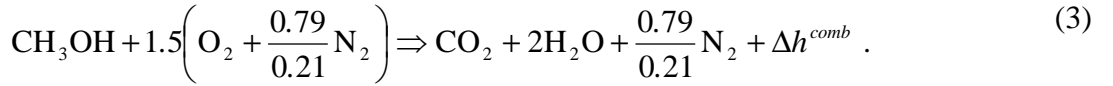
In the numerical model, the door into the compartment is enclosed with 1.2 m by 1.2 m by 0.8 m large additional volume. The purpose of this volume is to allow gases to move uninterrupted from and to the compartment. Therefore, "opening" boundary conditions were assigned to the volume boundaries except at the bottom, where the wall (no-slip) boundary conditions were implemented. The opening boundary conditions allow the fluid to cross the boundary in both directions by setting static pressure p_{stat} for the outgoing flow, and total pressure $p_{stat} + 0.5\rho v^2$ for the incoming flow.

The fluid flow is described with mass and momentum transport equations using the Favre-averaged form to better represent turbulence and changes in material composition (e.g. Cox [18]):

$$\partial_t \rho + \partial_j (\rho \bar{v}_j) = 0 \quad (1)$$

$$\partial_t (\rho \bar{v}_i) + \partial_j (\rho \bar{v}_j \bar{v}_i) = -\partial_i \bar{p} + \partial_j \left(\mu (\partial_j \bar{v}_i + \partial_i \bar{v}_j) - \frac{2}{3} \mu (\partial_l \bar{v}_l) \delta_{ji} \right) + g (\rho - \rho_{ref}) - \partial_j (\rho \overline{v_j' v_i'}) \quad (2)$$

The chemical reaction between the fuel and the air is modelled with a single step chemical reaction:



where $\Delta h^{comb} = 676.2$ kJ/mol is the combustion heat release. For transport of each component CH_3OH , O_2 , H_2O and CO_2 , a separate mass fraction transport equation is written:

$$\partial_t (\rho \bar{\xi}_c) + \partial_j (\rho \bar{v}_j \bar{\xi}_c) = \partial_j (\rho D_c \partial_j \bar{\xi}_c) + S_c^{comb} - \partial_j (\rho \overline{v_j' \xi_c'}) , \quad (4)$$

where S_c^{comb} is a mass source term due to the chemical reaction involving component c . The mass fraction of nitrogen is determined from the condition $\xi_i = 1$. The energy transport is modelled with a transport equation for static specific enthalpy:

$$\partial_t (\rho \bar{h}) - \partial_t \bar{p} + \partial_j (\rho \bar{v}_j \bar{h}) = \partial_j (k \partial_j \bar{T}) + \bar{v}_j \partial_j \bar{p} + S_c^{comb} \Delta h_c^{comb} + S^{rad} - \partial_j (\rho \overline{v_j' h_j'}) . \quad (5)$$

where beside the reaction energy release $S_c^{comb} \Delta h_c^{comb}$, radiation contribution S^{rad} has to be also taken into account.

To calculate eddy viscosity μ_t of turbulent flow, Shear Stress Transport (SST) model [19] is used. The model requires solution of a transport equation for turbulence kinetic energy k and for turbulence eddy frequency ω .

Using the obtained turbulence viscosity μ_t , Reynolds stresses, heat and mass fluxes are calculated as:

$$\overline{\rho v_j' v_i'} = -\mu_t 2S_{ij} + \frac{2}{3} \rho k \delta_{ij}, \quad \overline{\rho v_j' h'} = -\frac{\mu_t}{Pr_t} \partial_j \bar{h}, \quad \overline{\rho v_j' \xi_c'} = -\frac{\mu_t}{Sc_t} \partial_j \bar{\xi}_c. \quad (6)$$

3.1. Combustion modelling

Combustion of methanol jet in the air is modelled with the eddy-dissipation model (Magnussen and Hjertager [20]), based on the assumption that the chemical reaction is fast relative to the transport processes in the flow. The model assumes that the reaction rate may be related directly to the time required to mix reactants at the molecular level. Therefore, the level of turbulent mixing, which is defined with turbulence time scale $t_{flow} = k/\epsilon$, is a controlling condition for a combustion reaction. The other limiting factor of the combustion reaction is availability of fuel and oxygen. Thus, the following mathematical description of the reaction rate is used in the performed numerical simulations:

$$R^{comb} = C_A \frac{\epsilon}{k} \min \left(\frac{\bar{\xi}_{CH_3OH}}{\bar{v}'_{CH_3OH}}, \frac{\bar{\xi}_{O_2}}{\bar{v}'_{O_2}} \right), \quad (7)$$

where $C_A = 4.0$ is the empirical constant. The mass source term in the species transport equation (4) is then calculated as

$$S_c^{comb} = M_c (\bar{v}_c'' - \bar{v}_c') R^{comb}, \quad (8)$$

where \bar{v}_c' and \bar{v}_c'' are stoichiometric coefficients of reactants and products, respectively.

3.2. Thermal radiation modelling

Important heat transfer mechanism in the presented case is thermal radiation. In order to determine the radiation source S^{rad} due to volumetric absorption in each control volume as well as the radiation heat fluxes on the walls, the radiation transport was modelled using the Discrete Transport model (Shah [21]). All the walls in the simulation domain, were considered opaque and diffusive, with total emissivity $\epsilon = 0.9$.

Assuming isotropic scattering, thermal radiation equation can be simplified to

$$d_s I_\lambda(r, s) = -(K_{a\lambda} + K_{s\lambda}) I_\lambda(r, s) + K_a I_b(\lambda, T) + \frac{K_{s\lambda}}{4\pi} \int_{4\pi} I_\lambda(r, s') d\Omega' \quad (9)$$

Radiation intensity I_λ is then integrated along each ray from the boundaries of simulation domain assuming reasonable homogenous radiation intensity field:

$$I_\lambda(r, s) = I_{0\lambda} e^{-(K_{a\lambda} + K_{s\lambda})s} + I_{b\lambda} (1 - e^{-K_a s}) + K_{s\lambda} \bar{I}_\lambda \quad (10)$$

The first term represents the contribution due to absorption and out-scattering of the radiation leaving the boundary, the second term the emitted radiation, and the third term the in-scattering in each volume element.

To better represent radiative transport properties of combustion gas mixture, the multigrey gas formulation of Taylor and Foster [22] is used. Radiative properties of the mixture are expressed as a function of temperature and $p \cdot L$, which is the product of the partial pressure and the ray length. This functional dependence can be accurately correlated by assuming that the mixture behaves as a group of a sufficient number of grey gases. Therefore, for each grey gas, the radiation absorption coefficient is calculated as

$$K_{ag} = p \left(k_g (\bar{\zeta}_{H_2O} + \bar{\zeta}_{CO_2}) + k_{HCg} \bar{\zeta}_{CH_3OH} \right) \quad (11)$$

where k_g and k_{HCg} are empirical parameters for a given grey gas (Table I). They were obtained from the measured spectral data by Hadvig [23] and Beer et al. [24]. Note, that in the presented combustion case, the dominant emitters of radiation are carbon dioxide and water vapour.

In the performed numerical simulations, 4 grey gases were used in the multigrey gas formulation. For each grey gas, equation (10) is solved and partial radiation intensity I_g is obtained. In the same way, the radiation heat fluxes and, consequently, also the radiation source terms in the energy equation (5) are calculated for each gas separately:

$$q_{g,i}^{rad} = \int_{4\pi} I_g(r,s) \cos \varphi_i \cos \theta d\Omega \quad (12)$$

$$S_g^{rad} = -\partial_i q_{g,i}^{rad} \quad (13)$$

The resulting radiation heat fluxes are obtained by a weighted sum:

$$q_i^{rad} = \sum_{g=1}^4 a_g q_{g,i}^{rad} \quad (14)$$

where the coefficients a_g are represented as linear functions of temperature:

$$a_g = b_{1g} + 10^{-5} b_{2g} \bar{T} \quad (15)$$

The values of grey gas parameters b_{1g} and b_{2g} for the present case are given Table I.

Table I: Gray parameters for $p_{H_2O}/p_{CO_2} = 2$.

gas	k_g [$m^{-1} atm^{-1}$]	k_{HCg} [$m^{-1} atm^{-1}$]	b_{1g} [-]	b_{2g} [K^{-1}]
1	0.0	3.85	0.364	4.74E-05
2	0.69	0.0	0.266	7.19E-05
3	7.4	0.0	0.252	-7.41E-05
4	80.0	0.0	0.118	-4.52E-05

4. Semi-analytical model of the walls' thermal behaviour

The walls participate in the heat exchange process with interior of the fire enclosure as well with the surrounding environment. As figure 3 shows, the walls are exposed to convective heat flux q_c and thermal irradiation flux q_i , which is partly reflected back as q_r . The absorbed part of heat flow is further conducted through the walls into environment. As the internal side

of the walls gets hotter, the emitted flux q_e becomes also important. Moreover, these heat fluxes are time dependent, which further complicates thermal behaviour of the walls.

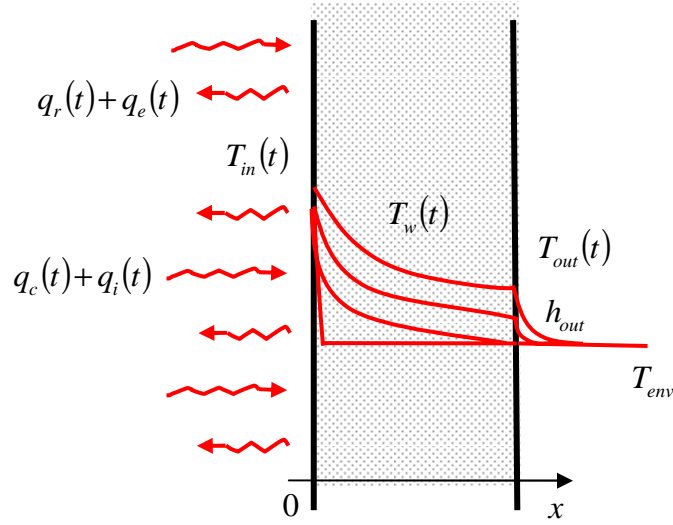


Figure 3 : Thermal model of the wall

The thermal effect of the walls onto heat transfer inside the enclosure can be modelled by a heat transfer coefficient h_w and a constant environmental temperature $T_{env} = 295$ K. To take into account the complex thermal behaviour, values of the heat transfer coefficient must vary along the walls as well as with time.

The heat transfer coefficient can be expressed with a temperature gradient inside the wall at the internal boundary:

$$h_w(t) = -k_w \frac{\partial_x T(t,0)}{\Delta T} \quad (16)$$

where $\Delta T = T_{in}(t) - T_{env}$. In order to determine $\partial_x T(t,0)$, temperature distribution inside the wall has to be calculated in each timestep by solving a diffusion equation with initial and boundary conditions:

$$\begin{aligned} \partial_t T &= \vartheta_w \partial_x \partial_x T \\ T(t^{n-1}, x) &= T_w^{n-1}, \quad T(t,0) = T_{in}(t), \quad -k_w \partial_x T(t,\delta) = h_{out}(T(t,\delta) - T_{env}) \end{aligned} \quad (17)$$

The values of wall thermal diffusivity ϑ_w and conductivity k_w were taken from the manufacturer's data for the enclosure insulation cladding (Fiberfax LD Duraboard). For

thermal diffusivity, a single value $\vartheta_w = 8.6 \cdot 10^8 \text{ m}^2/\text{s}$ was used, whereas for thermal conductivity, temperature dependent discrete values were approximated with a second order polynomial: $k_w = 1.3 \cdot 10^{-7} T'^2 + 2.9 \cdot 10^{-5} T' + 6.68 \cdot 10^{-2}$, where T' is the wall temperature in degrees Celsius (Tofilo et al. [1]).

The heat transfer coefficient at the external wall h_{out} is calculated for different wall orientations with simplified expressions:

$$h_{out} = 2.49(T(t, \delta) - T_{env})^{1/4} \text{ - for a horizontal wall facing up} \quad (18)$$

$$h_{out} = 1.31(T(t, \delta) - T_{env})^{1/4} \text{ - for a horizontal wall facing down}$$

$$h_{out} = 1.37(T(t, \delta) - T_{env})^{1/4} \text{ - for a vertical wall}$$

that were collected by Kothandaraman and Subramanyan [25].

In order to simplify further treatment and solution of the problem, the diffusion equation, initial and boundary conditions are scaled using the following relations:

$$\hat{x} = \frac{x}{\delta}, \quad \hat{t} = \frac{\vartheta}{\delta^2} dt, \quad \hat{T}(\hat{t}, \hat{x}) = \frac{T(t, x) - T_{env}}{T_{in} - T_{env}} \quad (19)$$

to obtain their dimensionless form

$$\begin{aligned} \partial_{\hat{t}} \hat{T} &= \partial_{\hat{x}} \partial_{\hat{x}} \hat{T} \\ \hat{T}(0, \hat{x}) &= \hat{T}_w^{n-1}, \quad \hat{T}(\hat{t}, 0) = 1, \quad -\partial_{\hat{x}} \hat{T}(\hat{t}, 1) = Bi_{out} \hat{T}(\hat{t}, 1) \end{aligned} \quad (20)$$

The dimensionless variables are marked with a caret symbol $\hat{}$ to be distinguish from the dimensional form of variables. Note that the internal wall temperature T_{in} is recalculated once per integration timestep and is treated as a constant in a single integration timestep.

Next, the temperature field is separated into a stationary and a transitional part: $T(t, x) = T_1(x) + T_2(t, x)$. The stationary part represents the temperature field after the initial transient, in the limit when $\hat{t} \rightarrow \infty$, whereas the transitional part time describes a time

dependent temperature deviation from the stationary state. As a result, the diffusion equation (20) is also split onto the stationary part:

$$\begin{aligned} \partial_{\hat{x}} \partial_{\hat{x}} \hat{T}_1 &= 0 \\ \hat{T}_1(0) &= 1, \quad -\partial_{\hat{x}} \hat{T}_1(1) = Bi_{out} \hat{T}_1(1) \end{aligned} \quad (21)$$

and the transient part

$$\begin{aligned} \partial_{\hat{t}} \hat{T}_2 &= \partial_{\hat{x}} \partial_{\hat{x}} \hat{T}_2 \\ \hat{T}_2(0, \hat{x}) &= \hat{T}_w^{n-1} - \hat{T}_1(\hat{x}), \quad \hat{T}_2(\hat{t}, 0) = 0, \quad -\partial_{\hat{x}} \hat{T}_2(\hat{t}, 1) = Bi_{out} \hat{T}_2(\hat{t}, 1) \end{aligned} \quad (22)$$

The solution of the stationary part (21) is

$$\hat{T}_1(\hat{x}) = 1 - \frac{Bi_{out}}{1 + Bi_{out}} \hat{x} \quad (23)$$

whereas, the solution of the transient part (22) can be found in the following form

$$\hat{T}_2(\hat{t}, \hat{x}) = e^{-\lambda^2 \hat{t}} (A \sin(\lambda \hat{x}) + B \cos(\lambda \hat{x})) \quad (24)$$

Using the boundary condition $\hat{T}_2(\hat{t}, 0) = 0$, equation (24) is further reduced to

$$\hat{T}_2(\hat{t}, \hat{x}) = A e^{-\lambda^2 \hat{t}} \sin(\lambda \hat{x}) \quad (25)$$

Taking into account the other boundary condition: $-\partial_{\hat{x}} \hat{T}_2(\hat{t}, 1) = Bi_{out} \hat{T}_2(\hat{t}, 1)$, an implicit expression for eigenvalues λ is obtained:

$$\lambda = -Bi_{out} \tan(\lambda) \quad (26)$$

The values of λ_i were calculated iteratively with Newton-Raphson method for the values of Bi_{out} between 0 and 5, and tabulated for later use.

The expressions for both parts of temperature field (23) and (25) are then summed:

$$\hat{T}(\hat{t}, \hat{x}) = 1 - \frac{Bi_{out}}{1 + Bi_{out}} \hat{x} + A e^{-\lambda_i^2 \hat{t}} \sin(\lambda_i \hat{x}) \quad (27)$$

To determine the value of coefficients A , the temperature field from the previous timestep is used as an initial condition $\hat{T}(0, \hat{x}) = \hat{T}^{n-1}$ in equation (27), which produces:

$$\hat{T}^{n-1} = 1 - \frac{Bi_{out}}{1 + Bi_{out}} \hat{x} + A \sin(\lambda_i \hat{x}) \quad (28)$$

The expression (28) is then multiplied with the functions $\sin(\lambda_j \hat{x})$ and integrated from 0 to 1:

$$\int_0^1 \left(\hat{T}^{n-1} - 1 + \frac{Bi_{out}}{1 + Bi_{out}} \hat{x} \right) \sin(\lambda_j \hat{x}) d\hat{x} = A \int_0^1 \sin(\lambda_i \hat{x}) \sin(\lambda_j \hat{x}) d\hat{x} \quad (29)$$

In matrix form, equation (29) is written as $J_j^{(1)} = A_j J_{ij}^{(2)}$, where the integrals $J_{ij}^{(2)}$ can be calculated analytically, but the integrals $J_j^{(1)}$ has to be evaluated numerically.

Using the orthogonality assumption of functions $\sin(\lambda_j \hat{x})$, the coefficients are calculated as

$$A_j = \frac{2J_j^{(1)}}{\left(1 - \frac{\sin(2\lambda_j)}{2\lambda_j} \right)} \quad (30)$$

Note that the functions $\sin(\lambda_j \hat{x})$ are not exactly orthogonal, although the assumption produces good results. Finally, the temperature field can be then expressed in its dimensional form as

$$T = T_{in}(t) - \Delta T \left[\left(\frac{Bi_{out}}{1 + Bi_{out}} \right) \frac{x}{\delta} - A_i e^{-\lambda_i^2 \frac{\delta}{\delta^2} dt} \sin \left(\lambda_i \frac{x}{\delta} \right) \right] \quad (31)$$

where $T_{in}(t)$ is the temperature on the internal side of the wall. Using the definition (16), the heat transfer coefficient is further calculated as

$$h_w(t) = \frac{k}{\delta} \left[\left(\frac{Bi_{out}}{1 + Bi_{out}} \right) - A_i \lambda_i e^{-\lambda_i^2 \frac{\delta}{\delta^2} dt} \right] \quad (32)$$

5. Computational implementation

The geometrical and physical model was set using ANSYS CFX software (ver. 10.0). The CFX code solves the system of Navier-Stokes equations on an unstructured numerical grid by implementing the Rhie-Chow interpolation scheme [26] between pressure and mass fluxes, which provides a reliable way to obtain smooth numerical solutions on co-located meshes (versus staggered meshes) without spurious oscillations. The presented analysis utilised in-built turbulence, combustion and radiation models available in the CFX code. The numerical methods implemented by the code are described in details in the online documentation (<http://www-waterloo.ansys.com/community>) and therefore will not be repeated here. The exceptions are the information particular to the presented case.

To perform the analysis, a numerical mesh with 168413 nodes and 793135 elements was generated. The majority of elements were tetrahedra, with slowly inflating layers of prisms aligned with the walls. The inflation layers are necessary to capture boundary layer effects. The first layer of nodes was only 2 mm away from a wall and in the viscous sublayer of the turbulent flow (i.e. $y^+ < 11.3$). Radiation intensities of the multigrey gas model I_g were calculated on a coarse mesh, which was obtained by joining 44 adjacent control volumes. For each of these volumes, radiation contribution was calculated from 24 rays in each angular direction. The integration time step was constant during the numerical simulations and set to 0.1 s.

The initial conditions of the performed numerical simulations represented the state in the experimental enclosure before the start of fuel inflow and combustion. Therefore, initially the fluid in the simulation domain consisted of air ($\psi_{O_2} = 0.21$ and $\psi_{N_2} = 0.79$) with zero velocity field and the temperature of 22 °C. The environmental temperature T_{env} needed to evaluate the wall heat transfer coefficient $h_w(t)$ was constant during the simulations and set to 22 °C.

At the beginning of the simulations, a table eigenvalues λ_i for a range of Biot number from 0 to 5 was generated. Then, at each timestep, a local value of Bi_{out} was calculated for each node on the walls, and the related set of eigenvalues λ_i was found from the table by interpolation. In all performed numerical simulations, 5 eigenvalues λ_i and eigenfunctions $\sin(\lambda_j \hat{x})$ were used

to approximate the temperature profile in the walls and to calculate the wall heat transfer coefficient $h_w(t)$. The calculation of temperature profile and $h_w(t)$ was performed at each timestep and for each node on the walls separately. The calculated values of $h_w(t)$ were then implemented directly in the numerical solver as a thermal boundary condition. Furthermore, the obtained temperature profile was used to evaluate the integral $J_j^{(1)}$, which was stored for the next timestep. This was the only variable stored between the time steps.

6. Results and discussion

For demonstration of the described computational procedure, only a limited set of results is presented for one of the walls. Figures 4-6 show the inside wall temperature distribution and heat fluxes at $t = 612$ s, when the fuel mass is at its peak.

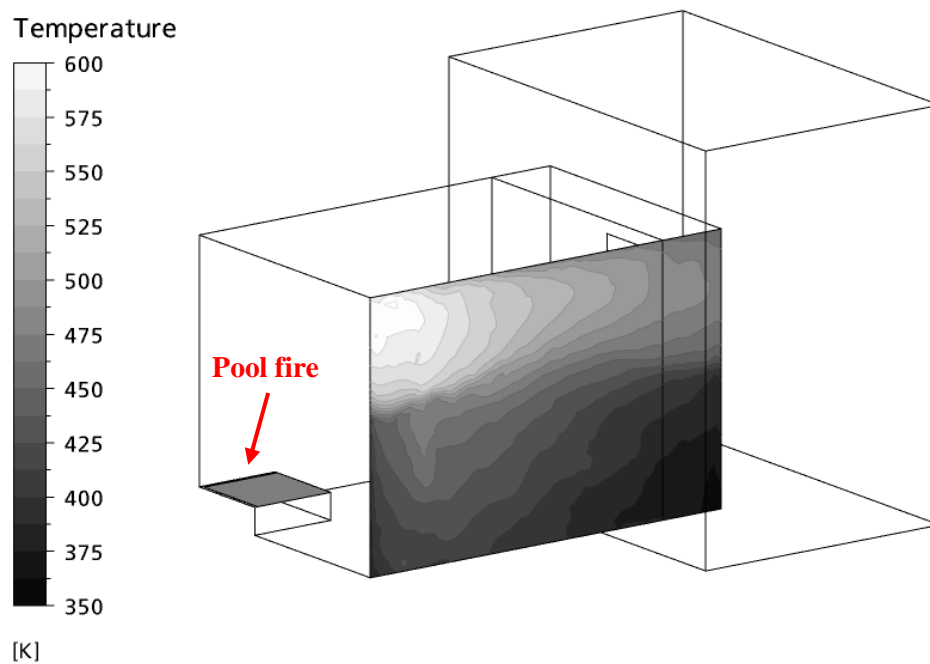


Figure 4: Inside wall temperature distribution $350\text{K} < T < 600\text{K}$ at $t = 612$ s

Buoyancy of hot gases due to fire and the restricted ventilation through the door cause formation of an upper - hot and a lower - cold layer. This separation fundamentally influences heat transfer in the enclosure. The temperature field in Figure 4 indicates this vertical division. The upper half of the wall is hotter than the lower half. The temperature maximum

that appears in the upper-left corner is due to impingement of a hot plume generated directly by the fire.

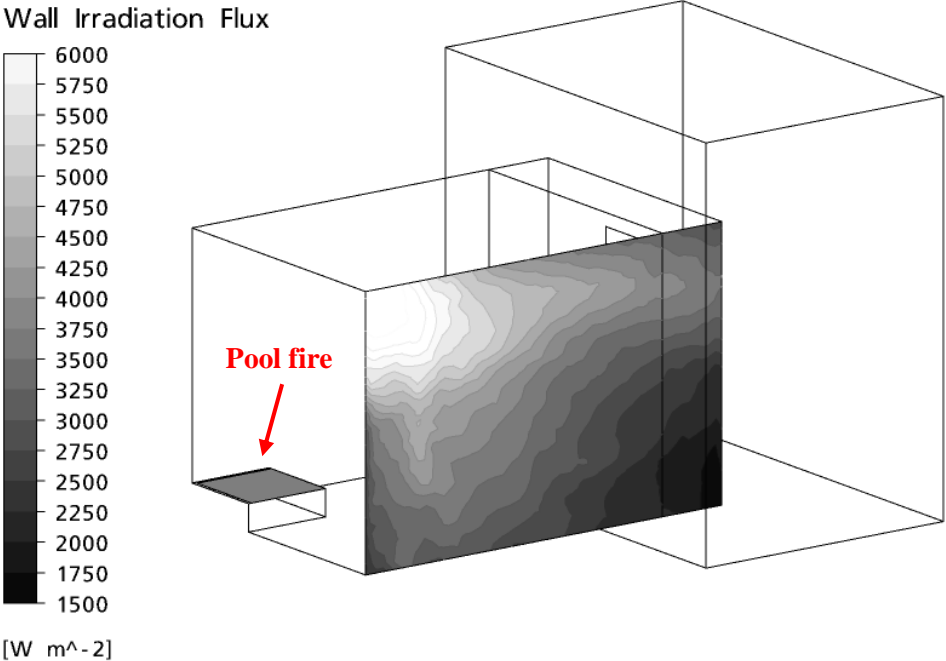


Figure 5: Wall irradiation flux $1500 \text{ W/m}^2 < q_i < 6500 \text{ W/m}^2$ at $t = 612 \text{ s}$

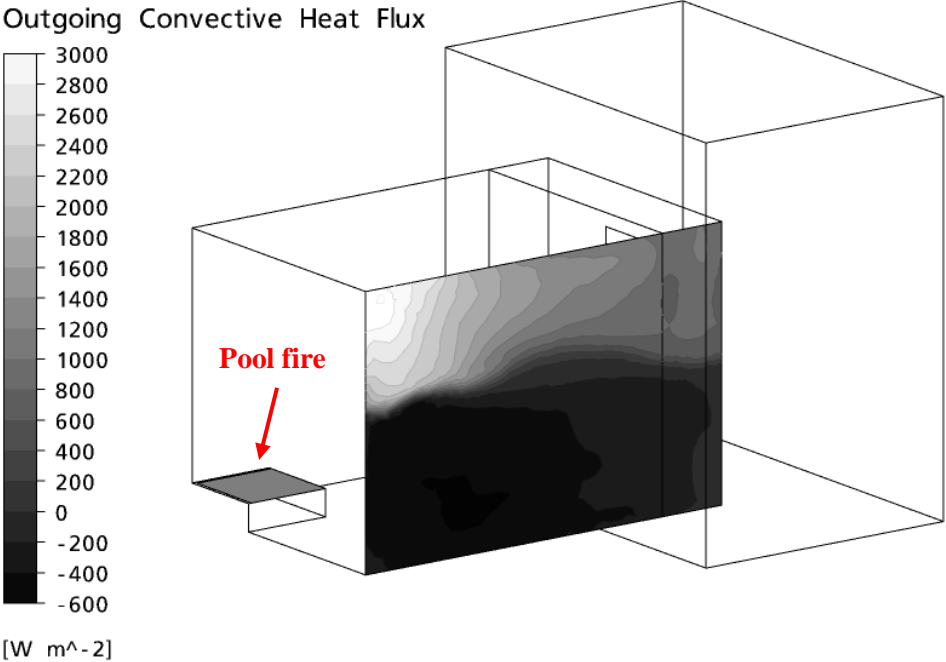


Figure 6: Outgoing convective heat flux $-600 \text{ W/m}^2 < q_c < 3000 \text{ W/m}^2$ at $t = 612 \text{ s}$

There are two mechanisms of heat transfer between the fire and the walls. Thermal radiation transports heat to the walls in a more uniform manner and it depends on temperature and distance from the dominant source. This can be observed in Figure 5, which shows distribution of the irradiation heat flux q_i . The other mechanism of heat transfer is thermal convection between the gases and the walls. Figure 6 shows how the hot and the cold layer of gases influence the distribution of convective heat flux in the enclosure.

Positive values of the outgoing convective heat flux q_c in the hot layer indicate that the wall is heated by the gases. The negative values of q_c reveal the opposite situation. Although, the lower half of the wall is heated by the irradiation, it is cooled by thermal convection as the temperature of gases in the cold layer is lower than the wall temperature.

The calculated gauge heat flux, which is the incoming irradiation and convective heat flux to a cold wall of the temperature T_{env} :

$$q_g = h_{in}(T_{gas} - T_{env}) + q_i \quad , \quad (33)$$

was compared with the experimental records (Tofilo et al. [1]) for 25 locations at the left wall as shown in Figure 1. The heat flux gauges were uniformly distributed across the wall.

To demonstrate the benefits of the developed semi-analytical wall treatment, additional numerical simulations were also performed for the adiabatic wall boundary conditions. Figures 7-11 show only a part of the results; they were obtained for the centre vertical row of the steel heat flux probes.

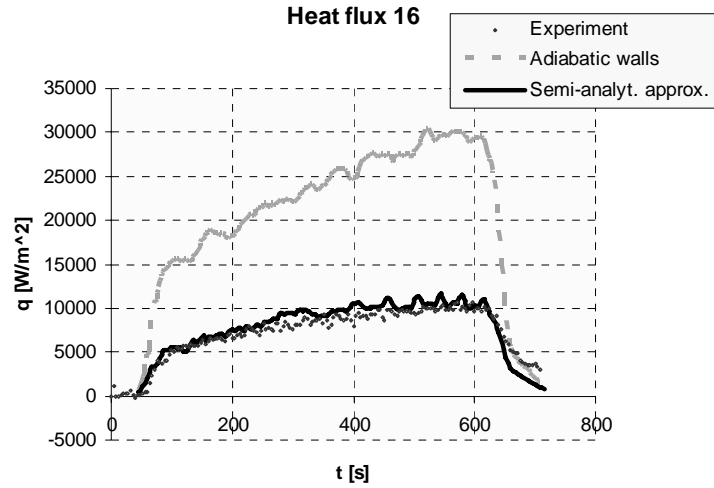


Figure 7: Gauge heat flux (38) from Probe 16 (Tofilo et al. [1])

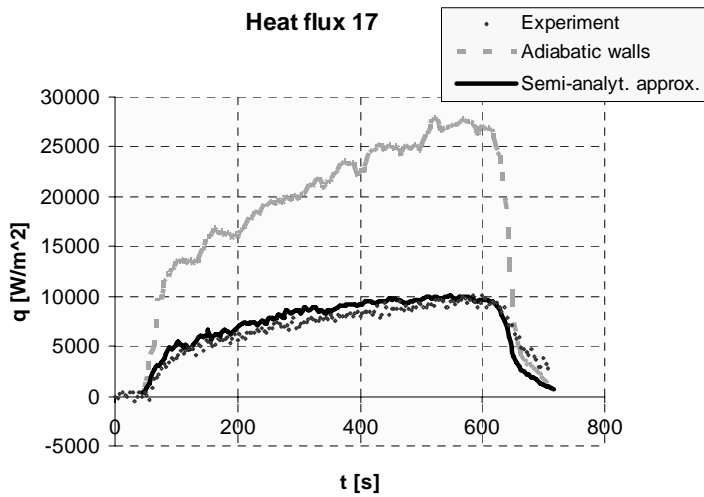


Figure 8: Gauge heat flux (38) from Probe 17 (Tofilo et al. [1])

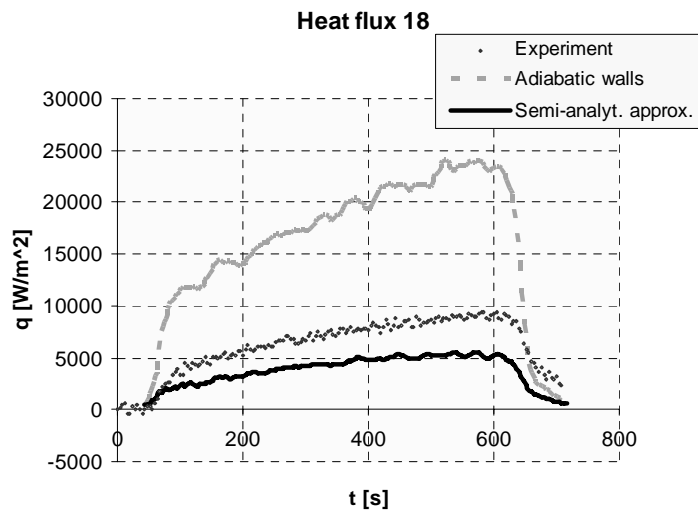


Figure 9: Gauge heat flux (38) from Probe 18 (Tofilo et al. [1])

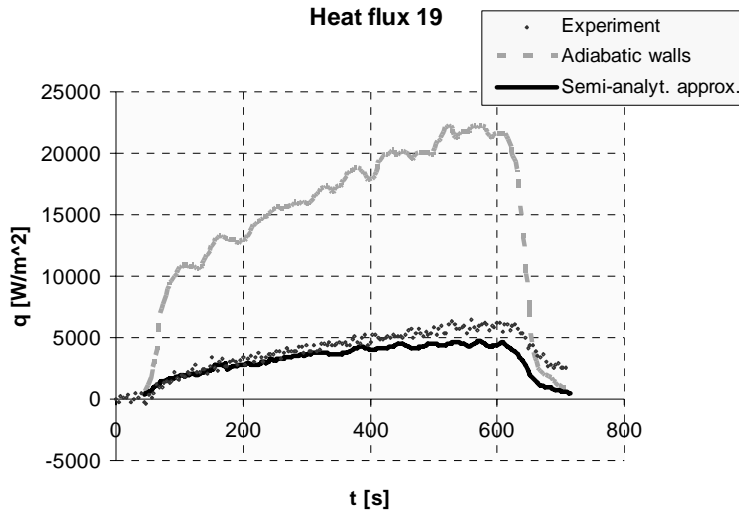


Figure 10: Gauge heat flux (38) from Probe 19 (Tofilo et al. [1])

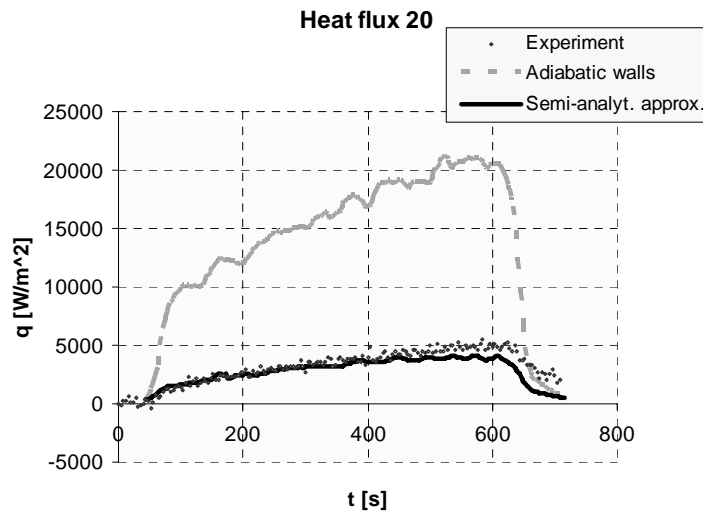


Figure 11: Gauge heat flux (38) from Probe 20 (Tofilo et al. [1])

The comparison in Figures 7-11 shows that the calculated gauge heat flux follows the experimental values for the whole recorded time interval, when semi-analytical approximation of wall heat transfer is used. Larger discrepancy can only be observed for Probe 18, where the calculated heat flux is lower than in the experiments (Tofilo et al. [1]). Namely, in the experiments, the probe is located inside the upper hot layer, whereas in the numerical simulation, it is left outside in the lower colder layer.

For comparison, when the adiabatic boundary conditions are used, the incoming heat flux is significantly overestimated.

7. Conclusions

A transient semi-analytical model of heat transfer through the walls was developed and coupled with a numerical model of fire in an enclosure to give an accurate prediction of heat flux on the enclosure walls. To take into account complex thermal behaviour, the temperature profile in the walls was reconstructed with a series of eigenfunctions in each simulation timestep for each grid node at the wall. The internal wall temperature served as a boundary condition on one side, whereas on the other side Cauchy boundary conditions were prescribed.

The presented analysis used turbulence, combustion and radiation models available in the CFX code. The numerical model of fire was based on the SST turbulence model (Menter [19]) and the eddy-dissipation combustion model (Magnussen and Hjertager [20]). For thermal radiation transport, the discrete transport model with the multigrey gas formulation (Taylor and Foster [22]) was used.

To validate the developed hybrid model, one of the experiments performed by Tofilo et al. [1] was used. The results show the hot-cold layer separation of gases. The walls are heated by irradiation from the hot plume and by thermal convection from the adjacent gases. The irradiation flux is much more uniformly distributed than the convective heat flux. As the fuel rate increases, the convective heat flux is positive in the upper - hotter layer and negative in the lower - colder layer. This indicates that the temperature of gases in the lower layer is below the wall temperature.

The comparison of calculated gauge heat fluxes for the adiabatic walls and for the semi-analytical approximation of heat conductive walls with the experimental results (Tofilo et al. [1]) clearly shows benefits of the developed semi-analytical technique. As the heat fluxes obtained with the coupled model closely follow the experimental data, the heat fluxes at the adiabatic walls significantly overestimate them.

Derivation and implementation of the presented transient semi-analytical technique is more complex in comparison to the numerical treatment of heat transfer in the walls. Nevertheless, there are some clear advantages that need to be emphasized. As the semi-analytical approach does not rely on a discretisation procedure, the accuracy of its solutions is independent of grid

spacing. Therefore, such semi-analytical technique is computationally less expensive and especially attractive for long transient calculations.

Acknowledgments

The present work was performed as a part of the project "Under-Ventilated Compartments Fires (FIRENET)" (Co. No. HPRN-CT-2002-00197). The project is supported by the EU Research Training Network FP5, which is gratefully acknowledged.

References

1. P. Tofilo, M.A. Delichatsios and G.W.H. Silcock, Effects of the Fuel Sootiness on the Wall Heat Fluxes in Enclosure Fires, in Gottuk, D. and Lattimer, B. (Eds.), Proceedings, 8th IAFSS Symposium, Beijing, China, pp. 987-998, 2005.
2. F.A. Jaber and S. James, A Dynamic Similarity Model for Large Eddy Simulation of Turbulent Combustion, *Physics of Fluids*, Vol. 10, No. 7, pp. 1775-1777, 1998.
3. X. Jiang and K.H. Luo, Dynamics and Structure of Transitional Buoyant Jet Diffusion Flames with Side-Wall Effects, *Combustion and Flame*, Vol. 133, pp. 29-45, 2003.
4. R. Hilbert, F. Tap, H. El-Rabii and D. Thévenin, D., Impact of Detailed Chemistry and Transport Models on Turbulent Combustion Simulations, *Progress in Energy and Combustion Science*, Vol. 30, pp. 61-117, 2004.
5. J. Janicka and A. Sadiki, Large Eddy Simulation of Turbulent Combustion Systems, *Proceedings of the Combustion Institute*, Vol. 30, pp. 537-547, 2005.
6. P. Koutmos, C Mavridis and D. Papailiou, Time-Dependent Computations of Turbulent Bluff-Body Diffusion Flames Close to Extinction, *International Journal of Numerical Methods for Heat & Fluid Flow*, Vol. 9 No. 1, pp. 39-59, 1999.

7. S. Kumar and G. Cox, Some Guidance on Correct Use of CFD Models for Fire Applications with Examples, Proceedings, INTERFLAM 2001, 9th International Fire Science & Engineering Conference, Edinburgh, Scotland, pp. 823-834, 2001.
8. N. Gobeau, H.S. Ledin and C.J. Lea, Guidance for HSE Inspectors: Smoke Movement in Complex Enclosed Spaces - Assessment of Computational Fluid Dynamics, HSL Report HSL/2002/29, Fire Explosion Group, Health and Safety Laboratory, Buxton, UK, 2002.
9. P.J. Stopford, Recent Applications of CFD Modelling in the Power Generation and Combustion Industries, Applied Mathematical Modelling, Vol. 26, pp. 351-374, 2002.
10. G.H. Yeoh, R.K.K. Yuen, E.W.M. Lee and S.C.P. Chueng, Fire and Smoke Distribution in a Two-Room Compartment Structure, International Journal of Numerical Methods for Heat & Fluid Flow, Vol. 12 No. 2, pp. 178-194, 2002.
11. J.R. Holman, Heat Transfer, 4th Edition, McGraw-Hill, New York, USA, 1976.
12. D. Drysdale, An Introduction to Fire Dynamics, John Wiley and Sons, Chichester, UK, 1990.
13. H.S. Carslaw and J.C. Jaeger, Conduction of Heat in Solids, 2nd Edition, Oxford University Press, UK, 1959.
14. A. Horvat and I. Catton, Application of Galerkin Method to Conjugate Heat Transfer Calculation, Numerical Heat Transfer, Part B: Fundamentals, Vol. 44, pp. 509-531, 2003.
15. A. Horvat and B. Mavko, Calculation of Conjugate Heat Transfer Problem with Volumetric Heat Generation Using the Galerkin Method, Applied Mathematical Modelling, Vol. 29, pp. 477-495, 2005.
16. A.D., Chernyshov, A.D., Solution of Nonstationary Problems of Heat Conduction for Curvilinear Regions by Direct Construction of Eigenfunctions, Journal of Engineering Physics and Thermophysics, Vol. 77, No. 2, pp. 445-453, 2004.

17. K. Pruess and Y. Zhang, A Hybrid Semi-Analytical and Numerical Method for Modeling Wellbore Heat Transmission, Paper LBNL-56824, Lawrence Berkeley National Laboratory, California, USA. 2004.
18. G. Cox, Combustion Fundamentals of Fire, Academic, London, UK, 1995.
19. F.R. Menter, Two-Equation Eddy-Viscosity Turbulence Models for Engineering Applications, AIAA Journal, Vol. 32, No. 8, 1994.
20. B.F. Magnussen and B.H. Hjertager, On Mathematical Modeling of Turbulent Combustion with Special Emphasis on Soot Formation and Combustion, Proceedings, The 16th Symp. (International) on Combustion, The Combustion Institute, Pittsburg, Pennsylvania, pp. 719–729, 1976.
21. N.G. Shah, New Method of Computation of Radiant Heat Transfer in Combustion Chambers, Ph.D. Thesis, Imperial College, London, United Kingdom, 1979.
22. P.B. Taylor and P.J. Foster, The Total Emissivities of Luminous and Non-Luminous Flames, International Journal of Heat and Mass Transfer, Vol. 17, pp. 1591-1605, 1974.
23. S. Hadvig, Gas Emissivity and Absorptivity, Journal of the Institute of Fuel, Vol. 43, pp. 129-135, 1970.
24. J.M. Beer, P.J. Foster and R.G. Siddall, Calculation Methods of Radiative Heat Transfer, HTFS Design Report No. 22, AEA Technology, UK, 1971.
25. C.P. Kothandaraman and S. Subramanyan, Heat and Mass Transfer Data Book, 3rd Ed. Wiley Eastern, New Delhi, India, p. 103, 1977.
26. C.M. Rhie and W.L. Chow, A Numerical Study of the Turbulent Flow Past an Isolated Airfoil with Trailing Edge Separation, AIAA Paper 82-0998. 1982.